Nanotechnology **27** (2016) 165203 (7pp)
doi:10.1088/0957-4484/27/16/165203

# Thickness-dependent charge transport in few-layer $MoS_2$ field-effect transistors

**Ming-Wei Lin, Ivan I Kravchenko, Jason Fowlkes, Xufan Li, Alexander A Puretzky, Christopher M Rouleau, David B Geohegan and Kai Xiao**

Center for Nanophase Materials Sciences, Oak Ridge National Laboratory, Oak Ridge, TN 37831, USA

E-mail: xiaok@ornl.gov

Received 11 December 2015, revised 1 February 2016
Accepted for publication 16 February 2016
Published 10 March 2016

**Abstract**

Molybdenum disulfide ($MoS_2$) is currently under intensive study because of its exceptional optical and electrical properties in few-layer form. However, how charge transport mechanisms vary with the number of layers in $MoS_2$ flakes remains unclear. Here, exfoliated flakes of $MoS_2$ with various thicknesses were successfully fabricated into field-effect transistors (FETs) to measure the thickness and temperature dependences of electrical mobility. For these $MoS_2$ FETs, measurements at both 295 K and 77 K revealed the maximum mobility for layer thicknesses between 5 layers (~3.6 nm) and 10 layers (~7 nm), with ~70 $cm^2 V^{-1} s^{-1}$ measured for 5 layer devices at 295 K. Temperature-dependent mobility measurements revealed that the mobility rises with increasing temperature to a maximum. This maximum occurs at increasing temperature with increasing layer thickness, possibly due to strong Coulomb scattering from charge impurities or weakened electron–phonon interactions for thicker devices. Temperature-dependent conductivity measurements for different gate voltages revealed a metal-to-insulator transition for devices thinner than 10 layers, which may enable new memory and switching applications. This study advances the understanding of fundamental charge transport mechanisms in few-layer $MoS_2$, and indicates the promise of few-layer transition metal dichalcogenides as candidates for potential optoelectronic applications.

S Online supplementary data available from stacks.iop.org/NANO/27/165203/mmedia

Keywords: $MoS_2$, field-effect transistor, metal insulator transition

(Some figures may appear in colour only in the online journal)

## 1. Introduction

Two-dimensional (2D) layered transition metal dichalcogenides (TMDs) have attracted intense attention as candidates to replace conventional Si technology [1–3]. Recent studies have demonstrated the potential of 2D layered materials for applications, such as field-effect transistors (FETs) [4–8], highly flexible transistors [9], and optoelectronics [10, 11]. Molybdenum disulfide ($MoS_2$), for example, has exhibited many unique optoelectronics properties, such as strong room temperature photoluminescence [12]. $MoS_2$ is covalently bonded in plane, allowing it to withstand high mechanical strain laterally, while weak Van der Waals interactions between layers lead to easy mechanical cleavage for tailoring layer number or aiding transfer during exfoliation techniques. $MoS_2$ has an indirect bandgap of ~1.3 eV in the bulk and a direct bandgap of ~1.8 eV as the material approaches a monolayer [13], making devices produced from thin layers of $MoS_2$ fundamentally different from their bulk counterparts in terms of their electrical and optical properties. $MoS_2$-based devices have recently been demonstrated, including FETs [7, 14–16], photo-transistors [12], low power electronics [17, 18] and gate-tuned superconductors [19]. Also $MoS_2$ exhibits a lack of inversion symmetry and a valley-split valence band, leading to a valley Hall effect that is promising for valley- or spin-tronic devices [20, 21]. Despite these advances in the field, the mobility of FETs based on mono- or few-layer $MoS_2$ is still relatively low compared to that found in the bulk. To address this shortcoming, many different approaches have recently been explored to enhance the mobility of 2D $MoS_2$ crystals, including the incorporation of high dielectric materials such as $HfO_2$ or $Al_2O_3$, or doping via the addition of a polymer electrolyte or ionic liquid on the top of the device [22–31]. However, despite these novel approaches few studies have addressed the crucial questions of the temperature dependent transport mechanisms and the optimal layer thickness for maximum mobility in 2D $MoS_2$ crystals.

Previous studies have presented the transport mechanisms of $MoS_2$ FET devices as corresponding to phonon-limited scattering at higher temperatures [7, 22], and variable range hopping (VRH) due to sulfur vacancies at lower temperatures [32]. The temperature dependence of mobility has been observed in either monolayer or few-layer $MoS_2$ crystals in previous reports [22, 25], however a systematic study of transport mechanisms versus layer thickness with temperature dependence has not yet been performed. It is essential to understand the underlying charge transport mechanisms for 2D $MoS_2$ with different number of layers (NLs) in order to assess the applicability of $MoS_2$ crystals for different potential electronic and optical applications.

In this study, mono- and few-layer $MoS_2$ crystals were exfoliated and transferred to $SiO_2/Si$ substrates using a conventional adhesive tape method, and $MoS_2$ FET devices were fabricated to measure thickness and temperature dependences of electrical mobility. A maximum mobility of ~70 $cm^2\,V^{-1}\,s^{-1}$ was observed at room temperature for 5L (~3.6 nm) flakes, however non-monotonic trends observed in the correlation between mobility and thickness both at room temperature and 77 K in the $MoS_2$ FET devices indicated that crystal layers with thicknesses between 5L (~3.6 nm) and 10L (~7 nm) were optimal for practical applications. The correlation of increasing temperature of peak mobility with increasing thickness is attributed to either the strong effect of Coulomb scattering or weakened in-plane electron–phonon interaction with increasing thickness. A metal–insulator transition (MIT) was observed for all thickness below 10L in our $MoS_2$ FET devices, with the limiting thickness of this phenomenon possibly related to the formation of a 2D electron gas with high carrier densities in $MoS_2$.

## 2. Experimental methods

The $MoS_2$ flakes were exfoliated from a bulk crystal onto a $SiO_2/Si$ wafer using adhesive tape. An optical microscope (Nikon LV150) was used to identify the location and estimated thickness of several flakes by noting their contrast. A Bruker Dimension Icon atomic force microscope (AFM) was then used to refine the thickness estimates. Raman spectroscopy (Renishaw Raman Spectrometer, 532 nm excitation source and 50X objective) was used to verify the characteristic peaks of the $MoS_2$ samples. The FETs were fabricated on a single wafer using electron beam lithography (JEOL 9300), simultaneously exposing all of the devices to the same processing step to ensure uniformity. Using electron beam evaporation, layers of 5 nm thick Ti and 30 nm thick Au were then deposited to form source/drain electrodes. Finally, the electrical properties of the devices were measured in a cryogenic probe system (~$1 \times 10^{-6}$ Torr base pressure) with a Keithley 4200 semiconductor analyzer using a two probe Si back-gate configuration.

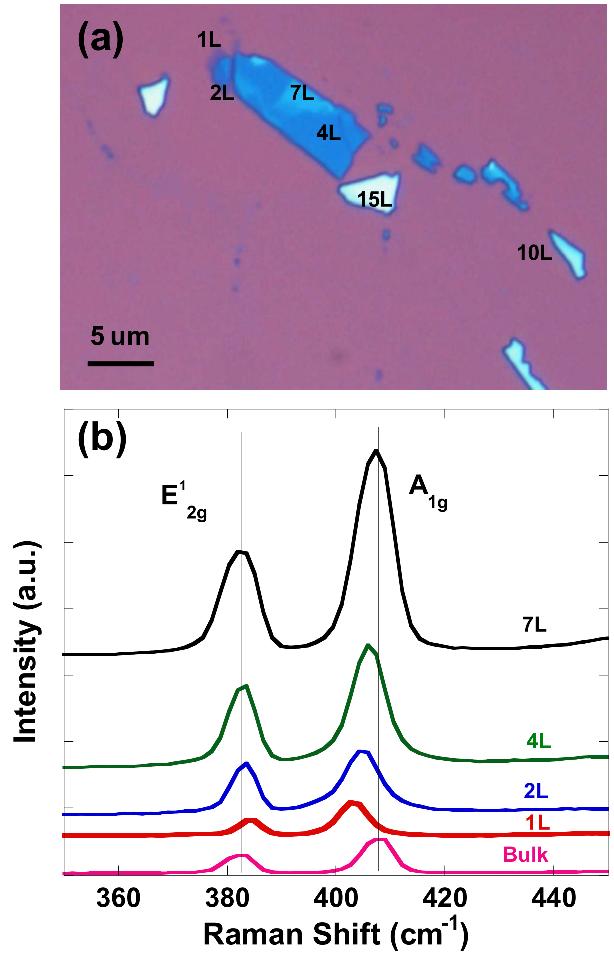


**Figure 1.** Optical microscope (OM) image and Raman spectrum of $MoS_2$ flakes using 532 nm excitation. (a) The OM image shows exfoliated $MoS_2$ flakes with various thicknesses as verified by AFM. Layer numbers are shown. (b) The Raman spectra show a shift of the characteristic peaks associated with in-plane ($E^1_{2g}$) and out-of-plane ($A_{1g}$) vibrations as thickness is reduced. A bulk spectrum is shown for reference.

## 3. Results and discussion

$MoS_2$ flakes were transferred to highly doped $Si/SiO_2$ (150 nm) wafers by repeated mechanical cleavage from a bulk crystal using adhesive tape. Figure 1(a) shows an optical microscope (OM) image of several $MoS_2$ flakes having 1, 2, 4, 7, 10, and 15 layers. Note that layer number was determined with AFM measurements. From the line scan of AFM images shown in figures S1(a) and (b), the thicknesses of

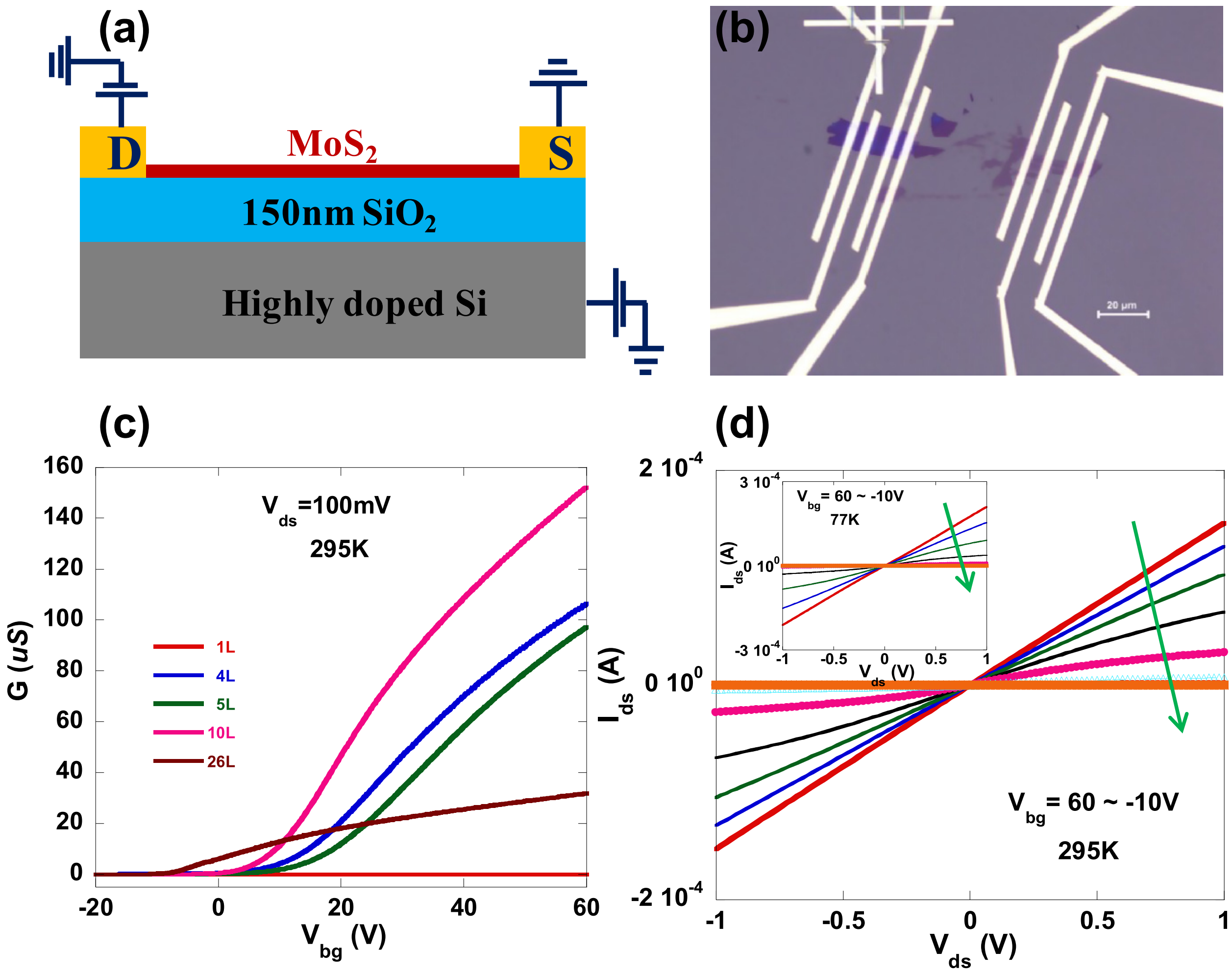


**Figure 2.** (a) Schematic of the $MoS_2$ FET devices that were fabricated on $SiO_2/Si$. (b) Optical microscopy image showing a plan view of the $MoS_2$ FET devices with electrodes. (c) Flake conductance versus back gate voltage at $V_{ds} = 100$ mV showing n-type behavior in all cases. (d) The $I_{ds}$–$V_{ds}$ curves for the 10 layer thick device demonstrating linear behavior for back gate voltage from −10 to 60 V, indicating ohmic contact both at room temperature and 77 K (inset).

flakes are 0.8 and 3 nm corresponding to mono and four layers, respectively. As shown in figure 1(b), Raman spectroscopy was performed to measure the characteristic peaks of $MoS_2$ associated with the $E^1_{2g}$ (in plane) and $A_{1g}$ (out of plane) vibrational modes, and measure their shifts with thickness. The $E^1_{2g}$ peak showed a red shift with increasing thickness, suggesting stacking-induced structural changes or the dominance of a long range Coulomb interaction in few layers $MoS_2$ [33]. In contrast, the $A_{1g}$ peak showed a blue shift with increasing thickness, owing to a higher force constant resulting from interlayer coupling [33, 34]. To ensure process uniformity, all the $MoS_2$ FETs were fabricated on a single wafer using standard electron beam lithography, yielding devices numbering in the tens with various thicknesses. Figure 2(a) shows a schematic of the $MoS_2$ FET devices and (b) shows an optical micrograph of a typical device in plan view.

The transport characteristics of the $MoS_2$ FET devices were measured from 295 K down to 77 K, and figure 2(c) is a plot of conductance ($G$) as a function of back gate voltage ($V_{bg}$) for several thicknesses. Note that all the devices exhibited n-*type* behavior, and conductance was defined as $G = I_{ds}/V_{ds}$, where $I_{ds}$ was the source–drain current, and $V_{ds}$ was the source–drain voltage (taken as 100 mV for all cases). The $I_{ds}$−$V_{ds}$ characteristics of a 10L (~7 nm) device as a function of $V_{bg}$ are shown in figure 2(d), while the inset indicates this linear behavior is maintained down to 77 K. Note that all the transport curves were measured at low bias $V_{ds} = 100$ mV minimize the effect of contact resistance, which was negligible in the present work. The field effect mobility was extracted from the linear region of the device transfer characteristics using the equation $\mu = \left(\frac{L}{WC_{ox}}\right)\left(\frac{\Delta G}{\Delta V_{bg}}\right)$, where $L$ was the channel length, $W$ was the channel width, and $C_{ox} = 2.3 \times 10^{-8}$ F cm$^{-2}$ was the capacitance between the channel and the back gate per unit area, and taken as $C_{ox} = \varepsilon_0\varepsilon_r/d_{ox}$, where $\varepsilon_0 = 8.85 \times 10^{-12}$ F m$^{-1}$, $\varepsilon_r = 3.9$ and $d_{ox} = 150$ nm. A mobility as high as 70 cm$^2$ V$^{-1}$ s$^{-1}$ was

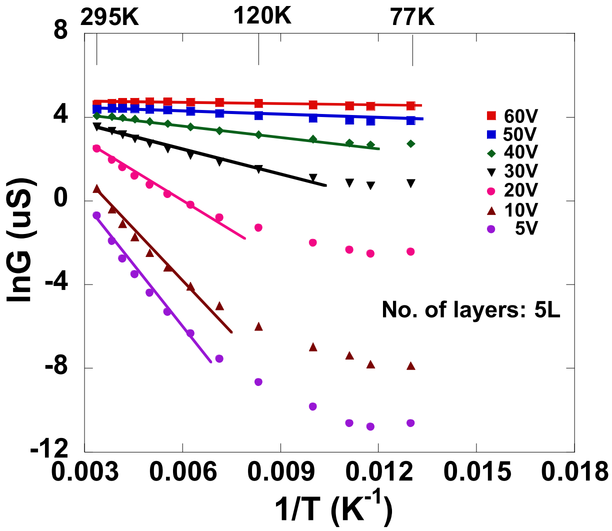


**Figure 3.** Arrhenius plot of conductance in a 5L device for back gate voltages ranging from 5 to 60 V. The solid lines are an aid to the eye, and show that for temperatures greater than ~120 K, the conductance is thermally activated, indicating charge transport is dominated by phonon limited scattering.

achieved at 295 K for a 5L device, which is in agreement with the value reported for few-layer devices using the same back gate geometry and two-probe measurement [35], and even higher than the 0.1–10 $cm^2 V^{-1} s^{-1}$ value reported for monolayer $MoS_2$ [7, 22]. This is mainly due to the higher density of states and lower Schottky barrier found in multilayer $MoS_2$. Although other reports stated the higher mobility was obtained by utilizing top-gating or dual-gating configuration for mono- and few-layer $MoS_2$ devices [7, 24, 25, 36, 37], it was beyond the scope of our study. At 77 K, a mobility as high as 110 $cm^2 V^{-1} s^{-1}$ was achieved for a 5L device. Figure 3 is a plot of conductance as a function of temperature for various back gate voltages for a 5L device, and indicates that charge transport for few-layer $MoS_2$ is a thermally activated process at high temperature—i.e., Arrhenius in nature. Consequently, phonon limited scattering is the dominant transport mechanism at high temperatures. Note that the measurement was also carried out for different thicknesses (see figure S2 for 4L and 12L devices (stacks.iop.org/NANO/27/165203/mmedia)), and these too were found to be in agreement with a thermally activated model. Although some reports have shown the phonon scattering mechanism dominating in high and low temperatures [22, 37, 38], the weaker temperature dependence noted in our case below 100 K and at low back gate voltage was associated with low carrier density, and transport in this temperature regime was possibly attributed to a hopping mechanism through localized states [32].

In order to elucidate how mobility changed with $MoS_2$ thickness, it was plotted as a function of $MoS_2$ thickness (1L to 26L) for two temperatures as in figures 4(a) and (b). Similar trends in mobility were also found by Das *et al* [23] and Li *et al* [39] at room temperature, leading them to conclude Coulomb scattering from charged impurities and a

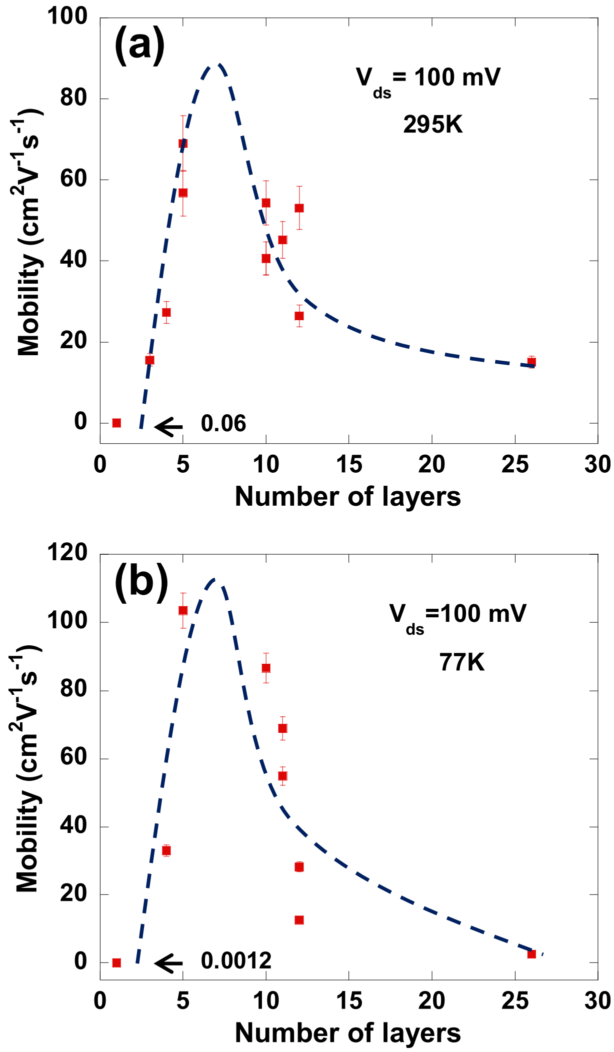


**Figure 4.** Mobility versus flake thickness for $MoS_2$ devices measured at 295 K (a) and 77 K (b), indicating an optimal thickness between 5L and 10L for maximum mobility in back-gated $MoS_2$ FET devices. The dashed blue line is a guide to the eye.

resistor network mechanism were responsible for the observed behavior. More specifically, as thickness increases, the effect of the substrate or charge impurities can be mitigated to some extent, leading to a mobility enhancement. However, the series resistance associated with an increasing number of interlayers [23, 40, 41] reverses this trend, and further increases in thickness reduces the mobility. At room temperature, our devices had a peak mobility of 60–70 $cm^2 V^{-1} s^{-1}$ for a thickness of 5L–10L. At low temperature, this value increased to 110 $cm^2 V^{-1} s^{-1}$ for a 5 layer device.

There are some reports [22, 25] indicating that the mobility of single- and few-layer $MoS_2$ devices peaks at 200 K and 160 K, respectively, but a systematic study of thickness dependence is not included. Although the charge transport with respect to different scattering mechanisms had been proposed, the surrounding dielectrics or reduced

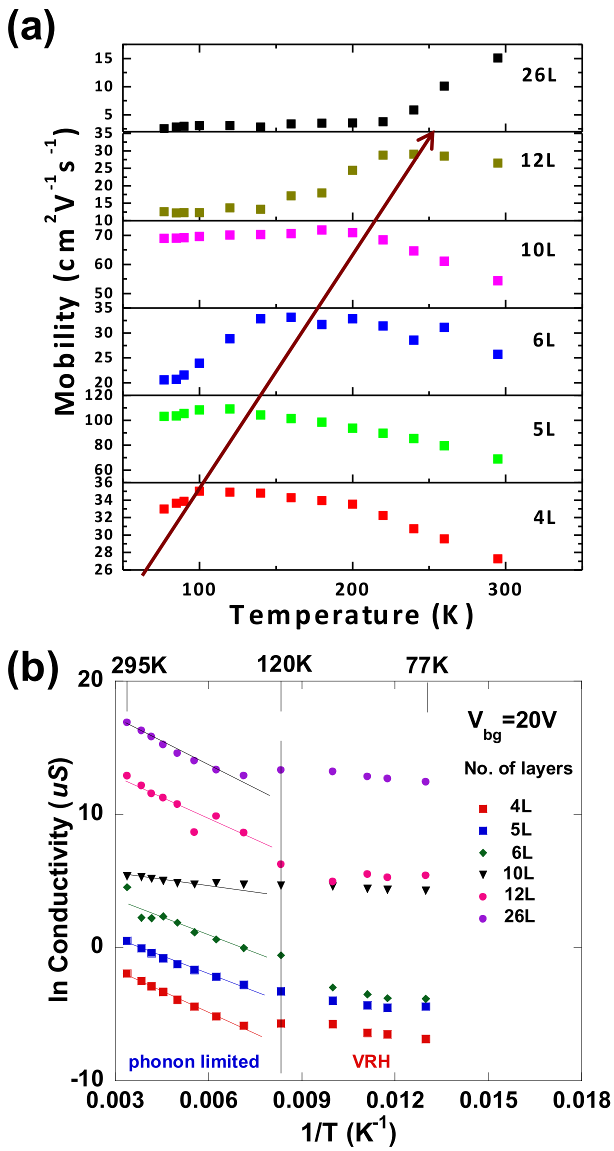


**Figure 5.** (a) Plot of mobility as a function of temperature for different device thicknesses, showing a transition in peak mobility temperature toward higher temperatures for increasing thickness. (b) Plot of conductivity versus temperature shows that phonon scattering dominates in high temperature regime (and low carrier density, $V_{bg} = 20$ V), while variable range hopping dominates for lower temperatures, giving a much weaker temperature dependence.

Coulomb scattering from charge impurities were considered critical factors for improved mobility [42]. To shed more light on the subject, we thermally cycled 4L, 5L, 6L, 10L, 12L and 26L thick devices, and plotted their mobility as function of temperature as in figure 5(a). As the figure shows, we found that the temperature at which the mobility peaks, increased with thickness. From Raman, the $E^1_{2g}$ peak corresponding to an in-plane vibrational mode was observed to red shift for increasing thickness, while the $A_{1g}$ peak associated with an out-of-plane vibrational mode was blue shifted. Since the mobility for higher temperatures was found to follow a thermally activated process—i.e., it was dominated by phonon limited scattering related to lattice vibrations—we can possibly attribute the shift in peak mobility temperature with thickness to weaker electron–phonon interactions in thicker devices. Coulomb scattering due to charged impurities may also weaken electron–phonon interactions in thicker $MoS_2$, again favoring a shift in the peak mobility temperature toward higher temperatures.

Kaasbjerg *et al* [43] have shown theoretically that the mobility due to optical and acoustic phonon scattering in monolayer $MoS_2$ increases with decreasing temperature, and follows the expression $\mu \sim T^{-\gamma}$, where the value of $\gamma$ is dependent on the scattering mechanism. By fitting the data in figure 5(a) in the high temperature regime, values for $\gamma$ were found to range from 0.5 to 0.7, and were smaller than the theoretical prediction of 1.69 for monolayer $MoS_2$, indicating that homo phonon mode quenching may be active in thicker devices, as was suggested in recent complimentary work on monolayer $MoS_2$ in top-gating configuration [22] and bilayer $MoS_2$ [27]. In order to shed additional light on the dominant mechanism in our $MoS_2$ FET devices, conductivity as a function of temperature was plotted with thickness for carrier densities ($n_{2D}$) in the range of $5.8 \times 10^{11}$–$3.9 \times 10^{12}$ cm$^{-2}$ at $V_{bg} = 20$ V as shown in figure 5(b). The carrier density is given by the expression $n_{2D} = C_{ox}\Delta V_{bg}/e$, where $C_{ox} = 2.3 \times 10^{-8}$ F cm$^{-2}$ is the capacitance, $\Delta V_{bg} = V_{bg} - V_{th}$ (threshold), and $e = 1.6 \times 10^{-19}$ C is the elementary charge. In the high temperature regime ($T > 120$ K), these curves follow a thermally activated process dominated by phonon limited scattering with a temperature dependence of $\sim T^{-1}$. Below 120 K, we attribute the weaker temperature dependence to variable range hopping (VRH) behavior due to low carrier densities or sulphur vacancies [32]. This hopping transport has been seen in graphene nanoribbons due to localized states at low temperatures [44].

Figure 6(a) shows the conductivity ($e^2/h$) of our 10L thick device as a function of back gate voltage ($V_{bg}$) and temperature. When gate voltages are below 40 V, the conductivity decreases with decreasing temperatures, indicating insulating behavior, whereas for gate voltages higher than 40 V, the temperature dependence is reversed, showing metallic behavior. The crossover from insulating to metallic conductivity is shown in more detail in figure 6(b). Note that this metal-insulation transition (MIT) behavior was only observed in our thinner devices (i.e., $<$10L). For thicker ones, the conductivity always decreases with decreased temperature (insulator behavior) at all gate biases (see figure S3 for 5L and 26L thick devices), suggesting a threshold thickness for the transition. It is interesting to note that a screening length of 5 nm (~7L) for unannealed $MoS_2$ FET devices has been reported, and was due to the trapping states induced by absorbed water molecules on the $MoS_2$ surface [45], analogous in our case to the possible production of a 2D electron gas with higher carrier density with less effect of localized states in devices thinner than 10 layers. With the encapsulation of high dielectric materials such as $HfO_2$, the MIT behavior has been observed for monolayer $MoS_2$ devices due

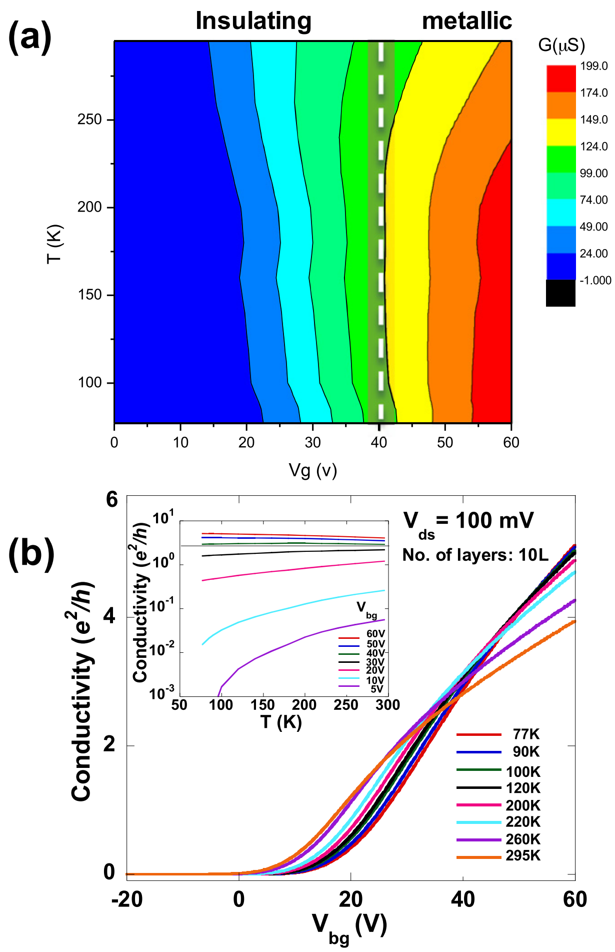


**Figure 6.** (a) Color plot of the conductivity as a function of temperature and gate voltage. (b) Conductivity as a function of gate voltage for different temperatures. The crossing around $V_{bg} \sim 40$ V indicates the change in temperature dependence. Inset shows the plot of temperature dependence of the two-terminal conductivity at different gate voltages from 5 to 60 V.

to impurities screening and high carrier densities [22]. In addition, the Ioffe–Regel criterion has been examined with the existence of a MIT for 2D semiconductors [46, 47]. According to the criterion, $k_F \cdot l_E \gg 1$ indicates a metallic phase, while $k_F \cdot l_E \ll 1$ indicates an insulating phase, where $k_F = (2\pi n_{2D})^{1/2}$ is the Fermi wave vector and $l_E = \hbar k_F \sigma / n_{2D} e^2$ is the mean free path of an electron. In our device, $k_F \cdot l_E = 2.84$ at the crossing point $V_{bg} = 40$ V (corresponding to a carrier density $n_{2D} = 4.7 \times 10^{12}\ \mathrm{cm}^{-2}$), which is in agreement with the theoretical prediction.

## 4. Conclusion

In conclusion, $MoS_2$ FET devices based on exfoliated mono- and few-layer crystals have been successfully fabricated, and conductance and mobility measurements have been made as a function of temperature. A mobility as high as $70\ \mathrm{cm}^2\ \mathrm{V}^{-1}\ \mathrm{s}^{-1}$ was achieved in a 5 layer thick device. Thickness-dependent mobility trends were observed at 295 K and 77 K, and provided an optimal thickness in the range of 5 layers to 10 layers for high performance applications. For each thickness, the mobility rises with increasing temperature to a peak. This peak mobility occurs at progressively increasing temperature with increasing thickness, which indicates that the Coulomb scattering due to charged impurities gradually dominates the charge transport in 2D $MoS_2$ crystals for thicker devices. Temperature-dependent conductivity measurements for different gate voltages reveal a metal-to-insulator transition for devices thinner than 10 layers. This study advances the understanding of fundamental charge transport mechanisms in few-layer $MoS_2$, and indicates the promise of few-layer transition metal dichalcogenides as candidates for potential optoelectronic applications.

## Acknowledgments

This research was conducted at the Center for Nanophase Materials Sciences (CNMS), which is a DOE Office of Science User Facility. MWL acknowledges support provided by a Laboratory Directed Research and Development award from Oak Ridge National Laboratory for device fabrication and characterization.

## References

[1] Novoselov K S, Jiang D, Schedin F, Booth T J, Khotkevich V V, Morozov S V and Geim A K 2005 Two-dimensional atomic crystals *Proc. Natl Acad. Sci.* **102** 10451–3
[2] Vogel E 2007 Technology and metrology of new electronic materials and devices *Nat. Nanotechnol.* **2** 25–32
[3] Yoon Y, Ganapathi K and Salahuddin S 2011 How good can monolayer $MoS_2$ transistors be *Nano Lett.* **11** 3768–73
[4] Fang H, Chuang S, Chang T C, Takei K, Takahashi T and Javey A 2012 High-performance single layered $WSe_2$ p-FETs with chemically doped contacts *Nano Lett.* **12** 3788–92
[5] Chamlagain B *et al* 2014 Mobility improvement and temperature dependence in $MoSe_2$ field-effect transistors on parylene-c substrate *ACS Nano* **8** 5079–88
[6] Podzorov V, Gershenson M E, Kloc C, Zeis R and Bucher E 2004 High-mobility field-effect transistors based on transition metal dichalcogenides *Appl. Phys. Lett.* **84** 3301–3
[7] Radisavljevic B, Radenovic A, Brivio J, Giacometti V and Kis A 2011 Single-layer $MoS_2$ transistors *Nat. Nanotechnol.* **6** 147–50
[8] Chuang H-J *et al* 2014 High mobility $WSe_2$ p- and n-type field-effect transistors contacted by highly doped graphene for low-resistance contacts *Nano Lett.* **14** 3594–601
[9] Pu J, Yomogida Y, Liu K-K, Li L-J, Iwasa Y and Takenobu T 2012 Highly flexible $MoS_2$ thin-film transistors with ion gel dielectrics *Nano Lett.* **12** 4013–7
[10] Eda G and Maier S A 2013 Two-dimensional crystals: managing light for optoelectronics *ACS Nano* **7** 5660–5
[11] Bernardi M, Palummo M and Grossman J C 2013 Extraordinary sunlight absorption and one nanometer thick photovoltaics using two-dimensional monolayer materials *Nano Lett.* **13** 3664–70

[12] Yin Z *et al* 2011 Single-layer $MoS_2$ phototransistors *ACS Nano* **6** 74–80
[13] Mak K F, Lee C, Hone J, Shan J and Heinz T F 2010 Atomically thin $MoS_2$: a new direct-gap semiconductor *Phys. Rev. Lett.* **105** 136805
[14] Ghatak S, Pal A N and Ghosh A 2011 Nature of electronic states in atomically thin $MoS_2$ field-effect transistors *ACS Nano* **5** 7707–12
[15] Han L and Ye P D 2012 $MoS_2$ dual-gate MOSFET with atomic-layer-deposited $Al_2O_3$ as top-gate dielectric *IEEE Electron Dev. Lett.* **33** 546–8
[16] Lembke D and Kis A 2012 Breakdown of high-performance monolayer $MoS_2$ transistors *ACS Nano* **6** 10070–5
[17] Fontana M, Deppe T, Boyd A K, Rinzan M, Liu A Y, Paranjape M and Barbara P 2013 Electron–hole transport and photovoltaic effect in gated $MoS_2$ Schottky junctions *Sci. Rep.* **3** 1634
[18] Kim S *et al* 2012 High-mobility and low-power thin-film transistors based on multilayer $MoS_2$ crystals *Nat. Commun.* **3** 1011
[19] Ye J T, Zhang Y J, Akashi R, Bahramy M S, Arita R and Iwasa Y 2012 Superconducting dome in a gate-tuned band insulator *Science* **338** 1193–6
[20] Ross J S *et al* 2013 Electrical control of neutral and charged excitons in a monolayer semiconductor *Nat. Commun.* **4** 1474
[21] Wu S *et al* 2013 Electrical tuning of valley magnetic moment through symmetry control in bilayer $MoS_2$ *Nat. Phys.* **9** 149–53
[22] Radisavljevic B and Kis A 2013 Mobility engineering and a metal–insulator transition in monolayer $MoS_2$ *Nat. Mater.* **12** 815–20
[23] Das S, Chen H-Y, Penumatcha A V and Appenzeller J 2012 High performance multilayer $MoS_2$ transistors with scandium contacts *Nano Lett.* **13** 100–5
[24] Lin M-W *et al* 2012 Mobility enhancement and highly efficient gating of monolayer $MoS_2$ transistors with polymer electrolyte *J. Phys. D: Appl. Phys.* **45** 345102
[25] Perera M M *et al* 2013 Improved carrier mobility in few-layer $MoS_2$ field-effect transistors with ionic-liquid gating *ACS Nano* **7** 4449–58
[26] Lembke D, Allain A and Kis A 2015 Thickness-dependent mobility in two-dimensional $MoS_2$ transistors *Nanoscale* **7** 6255–60
[27] Baugher B W H, Churchill H O H, Yang Y and Jarillo-Herrero P 2013 Intrinsic electronic transport properties of high-quality monolayer and bilayer $MoS_2$ *Nano Lett.* **13** 4212–6
[28] Shi Y *et al* 2012 van der Waals epitaxy of $MoS_2$ layers using graphene as growth templates *Nano Lett.* **12** 2784–91
[29] Liu H, Si M, Najmaei S, Neal A T, Du Y, Ajayan P M, Lou J and Ye P D 2013 Statistical study of deep submicron dual-gated field-effect transistors on monolayer chemical vapor deposition molybdenum disulfide films *Nano Lett.* **13** 2640–6
[30] Liu K-K *et al* 2012 Growth of large-area and highly crystalline $MoS_2$ thin layers on insulating substrates *Nano Lett.* **12** 1538–44
[31] Schmidt H *et al* 2014 Transport properties of monolayer $MoS_2$ grown by chemical vapor deposition *Nano Lett.* **14** 1909–13
[32] Qiu H *et al* 2013 Hopping transport through defect-induced localized states in molybdenum disulphide *Nat. Commun.* **4** 2642
[33] Li H, Zhang Q, Yap C C R, Tay B K, Edwin T H T, Olivier A and Baillargeat D 2012 From bulk to monolayer $MoS_2$: evolution of Raman scattering *Adv. Funct. Mater.* **22** 1385–90
[34] Lee C, Yan H, Brus L E, Heinz T F, Hone J and Ryu S 2010 Anomalous lattice vibrations of single- and few-layer $MoS_2$ *ACS Nano* **4** 2695–700
[35] Wang H *et al* 2012 Integrated circuits based on bilayer $MoS_2$ transistors *Nano Lett.* **12** 4674–80
[36] Fuhrer M S and Hone J 2013 Measurement of mobility in dual-gated $MoS_2$ transistors *Nat. Nanotechnol.* **8** 146–7
[37] Wang Q H, Kalantar-Zadeh K, Kis A, Coleman J N and Strano M S 2012 Electronics and optoelectronics of two-dimensional transition metal dichalcogenides *Nat. Nanotechnol.* **7** 699–712
[38] Jariwala D, Sangwan V K, Lauhon L J, Marks T J and Hersam M C 2014 Emerging device applications for semiconducting two-dimensional transition metal dichalcogenides *ACS Nano* **8** 1102–20
[39] Li S-L *et al* 2013 Thickness-dependent interfacial coulomb scattering in atomically thin field-effect transistors *Nano Lett.* **13** 3546–52
[40] Na J *et al* 2014 Separation of interlayer resistance in multilayer $MoS_2$ field-effect transistors *Appl. Phys. Lett.* **104** 233502
[41] Li S-L, Komatsu K, Nakaharai S, Lin Y-F, Yamamoto M, Duan X and Tsukagoshi K 2014 Thickness scaling effect on interfacial barrier and electrical contact to two-dimensional $MoS_2$ layers *ACS Nano* **8** 12836–42
[42] Ma N and Jena D 2014 Charge scattering and mobility in atomically thin semiconductors *Phys. Rev.* X **4** 011043
[43] Kaasbjerg K, Thygesen K S and Jacobsen K W 2012 Phonon-limited mobility in single-layer $MoS_2$ from first principles *Phys. Rev.* B **85** 115317
[44] Han M Y, Brant J C and Kim P 2010 Electron transport in disordered graphene nanoribbons *Phys. Rev. Lett.* **104** 056801
[45] Li Y, Xu C-Y and Zhen L 2013 Surface potential and interlayer screening effects of few-layer $MoS_2$ nanoflakes *Appl. Phys. Lett.* **102** 143110
[46] Gurvitch M 1981 Ioffe-Regel criterion and resistivity of metals *Phys. Rev.* B **24** 7404–7
[47] Graham M R, Adkins C J, Behar H and Rosenbaum R 1998 Experimental study of the Ioffe-Regel criterion for amorphous indium oxide films *J. Phys.: Condens. Matter* **10** 809